Structural Disorder in the α Form of Isotactic Polypropylene

Finizia Auriemma,* Odda Ruiz de Ballesteros, Claudio De Rosa, and Paolo Corradini

Dipartimento di Chimica, Università degli Studi di Napoli "Federico II", via Mezzocannone, 4-80134 Napoli, Italy

Received February 16, 2000; Revised Manuscript Received July 10, 2000

ABSTRACT: A detailed analysis of the Bragg as well as of the diffuse X-ray diffraction scattering of isotactic polypropylene (i-PP) fiber samples, suitably crystallized in the α form under different conditions, is reported. A limit-ordered (α_2 form) and a limit-disordered (α_1 form) model structure have been described to account for the features of the experimental X-ray diffraction profiles of i-PP samples prepared in the α form. The disorder consists of the statistical occupation of the lattice sites of isomorphous helices having opposite up/down orientations. Depending on the conditions of crystallization, intermediate-disordered modifications between the limit-ordered and the limit-disordered, can be obtained. The analysis of the Bragg contribution to the X-ray diffraction scattering of isotactic polypropylene samples crystallized in the α form provides direct quantitative information regarding the amount of up/down disorder, whereas the analysis of the diffuse scattering subtending the Bragg reflections in the case of oriented samples may provide detailed information on the development of the up/down disorder within the unit cell. Fiber samples annealed at high temperatures (∼170 °C), hence recrystallized slowly, and thus nearer to thermodynamic equilibrium, show X-ray diffraction patterns very close to that of the ideal limit-ordered model structure for the α form (α_2 form). Almost perfect order is maintained inside the bilayers, as in the limit-ordered structural model, and only 5−10% of defects in the relative orientation (up or down) of the helices belonging to adjacent bilayers along *b* is probably present. The presence of this kind of defect is consistent with the chain-folding scheme proposed in past literature. In the case of unannealed fiber samples, a large amount of up/down disorder is also present within the bilayers, giving rise, in the case of samples crystallized at lower temperatures, to situations very close to the limit-disordered model structure. We assume that the chain folding might not develop according to the scheme proposed in the literature for kinetic reasons.

Introduction

Isotactic polypropylene (i-PP), one of the most important semicrystalline commercial polymers, presents a complex polymorphism in the solid state, complicated by the presence of disorder. Three crystalline forms have been identified so far, named α, *β*, and *γ*, and a mesomorphic form.[1−9] They all are characterized by chains in a 3_1 $(TG)_n$ helical conformation, where T and G stand for backbone torsion angles in *trans* and *gauche* states, respectively.

The crystalline α form is generally obtained from melt-crystallization procedures and in drawn fibers.[10] Depending on the thermal and mechanical history, either melt-crystallized samples or drawn fibers, may present different degrees of structural disorder, indicating that they are crystallized in modifications, which can usefully be considered as intermediate between two ideal forms, the limit-ordered and the limit-disordered model structures.[11]

As first proposed by Natta and Corradini[1] and confirmed by successive studies,[2−4] the α form of i-PP can be described in terms of a monoclinic unit cell (*b* unique axis, chain axis $c = 6.5$ Å), containing four chains in a 3_1 helical conformation. Left- and right-handed helices, schematized as triangles in the projection perpendicular to *c* of Figure 1, are packed in the unit cell in such a way that isochiral chains related by a translation vector $\mathbf{t}_1 = \mathbf{a}$ are piled along *a* forming *a*−*c* rows of parallel chains, with the chains belonging to adjacent *a*−*c* rows stacked along *b* being enantiomorphous. A pair of adjacent *a*−*c* rows (delimited by the vertical dashed lines in Figure 1) is named a bilayer; within the bilayers,

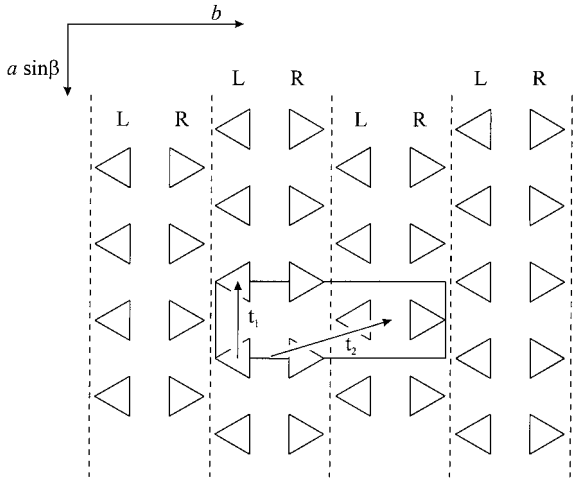

Figure 1. Mode of packing of right- (R) and left- (L) handed 3/1 helices (schematized as triangles) viewed along the *c* axis in the α form of i-PP. The vertical dashed lines delimit bilayers. $\mathbf{t}_1$ and $\mathbf{t}_2$, the translation vectors relating consecutive chains along *a* and consecutive bilayers along *b*, respectively, are indicated.

the helices face each other along *b* side by side. As shown in Figure 1, couples of consecutive bilayers along *b* are stacked through the translation vector $\mathbf{t}_2 = \mathbf{a}/2 + \mathbf{b}/2$.

Long-range disorder may be present in the structure, related to the possibility of occupation of the lattice sites of helices of the same chirality, but with the opposite orientation of the chain axis. This directional property is common to all isotactic vinyl polymers, and involves,

10.1021/ma0002895 CCC: $19.00
Published on Web 10/21/2000

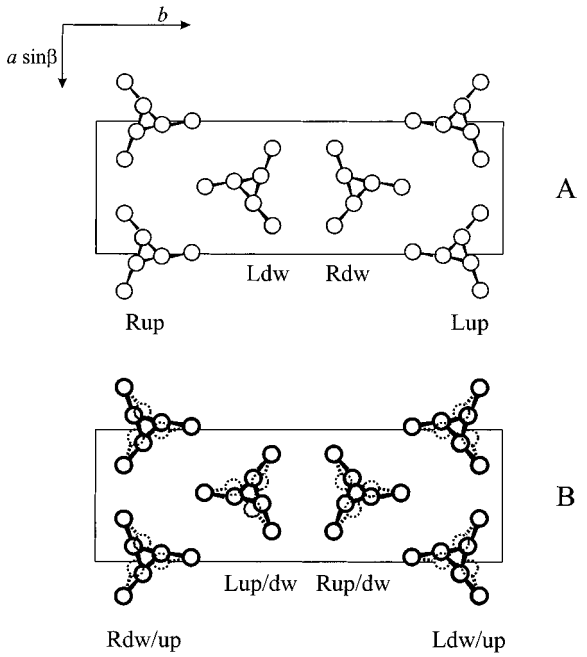

Figure 2. Model of packing of i-PP in the α form in the (A) limit-ordered (space group $P2_1/c$) and (B) limit-disordered (space group C2/*c*) model structures. In the limit-ordered model structure (α_2 form), each bilayer of isoclined chains is anticlined with respect to the adjacent bilayers; in the limit-disordered model structure (α_1 form), a complete disorder corresponding to a statistical substitutional of up and down helices occurs.

in the case of a $(TG)_n$ or a $(GT)_n$ helical conformation, a difference in the *z* coordinate (the *z* axis being assumed parallel to the chain axis) between the first atom of the lateral group and the main-chain tertiary atom; the difference between the two coordinates may be all positive or all negative for the same chain, depending on the orientation of the chain axis relative to an absolute reference frame. Correspondingly, the two orientations differing by a 180° rotation around an axis perpendicular to the chain axis, are called "up" or "down". Couples of chains both up or both down are said isoclined; otherwise, they are said to be anticlined.[12]

As shown in Figure 2A, in the limit-ordered (long-range-ordered) model structure, the $a-c$ rows of chains within the bilayers are related by a glide plane symmetry *c*, perpendicular to *b*, and the helices are all isoclined. The chains belonging to a given bilayer are anticlined with respect to those belonging to the adjacent bilayers (space group $P2_1/c$, unit cell parameters $a = 6.65$ Å, $b = 20.73$ Å, $c = 6.50$ Å, $\beta = 98.67°$).[3] In the limit-disordered (long-range-disordered) model structure, each lattice site is occupied at chance by helices of the appropriate chirality that are up or down. This full up/down disorder can be described in terms of the statistical space group $C2/c$[1] (see Figure 2B). According to the nomenclature proposed by Hikosaka and Seto, the limit-ordered and the limit-disordered model structures are named α_2 and α_1,[3] respectively.

Intermediate situations of disorder can arise because local correlations in the relative orientation of adjacent helices might be maintained. The degree of disorder, which depends on the crystallization conditions and the thermal history of the samples,[13−16] implies significant variations in the relative intensity of the Bragg reflections in the X-ray diffraction patterns. As indeed already outlined in the literature, i-PP samples that are well-crystallized[15] or annealed[13,14] at high temperature (i.e., close to the melting temperature[13]) present sharp and narrow *hkl* reflections with $h + k = 2n + 1$; this indicates that the samples are characterized by a structure very close to the limit-ordered form (α_2 form). For samples crystallized or annealed at low temperatures, such reflections become weak and broad, whereas those with $h + k = 2n$ remain narrow and sharp.[13,14] When the Bragg *hkl* reflections with $h + k = 2n + 1$ are completely absent, the structure is very close to the limit-disordered (C-centered) form (α_1 form). Moreover, the diffraction intensity subtending the Bragg reflections (diffuse scattering) increases with increasing degree of disorder and assumes characteristic shapes along the layer lines in oriented samples. The localization of such diffuse scattering on the layer lines is indicative of long-range positional up/down disordering of the chains.

Hikosaka and Seto,[3] in order to explain the fluctuations on the Bragg intensities, proposed a model in which ordered domains ($P2_1/c$), upon thermal treatments, develop inside previously disordered ($C2/c$) domains, so that, in the intermediate forms, regions with the α_1 and α_2 structures can coexist in various amounts within the same crystal. In this framework, Corradini et al.[16] suggested a limit-intermediate model in which the up/down disorder develops along one direction only. More precisely, a perfect order in the relative (up/down) orientation of the macromolecules is maintained within the bilayer according to the $P2_1/c$ model structure; the chains belonging to adjacent bilayers stacked along *b* have probability *p* of being anticlined and probability $(1 - p)$ of being isoclined. This model is in agreement with the indication of Mencik[2] that the *b*-axis direction is the most likely direction to show irregularities in the ideal sequence of chain molecules required by pure $P2_1/c$ symmetry. However, this kind of disorder is not sufficient to explain the magnitude and shape of the diffuse scattering present in the case of i-PP samples not crystallized at high temperatures, which usually show X-ray diffraction pattern features that are intermediate between those of the limit-ordered and the limit-disordered model structures.

In this paper, a detailed analysis of the Bragg as well as of the diffuse X-ray diffraction scattering of suitably prepared i-PP samples in the α form is performed for the first time. The experimental X-ray diffraction patterns are compared with those calculated for model structures involving various degrees and patterns of up/down (long-range) disorder. The energy cost of defects resulting in the occupation of lattice sites by helices with the wrong orientation with respect to the limit-ordered α_2 form is evaluated and correlated to the degree of structural disorder, which is observed in the examined samples.

Experimental Section

i-PP pellets were kindly furnished by Montell Polyolefins (Ferrara, Italy) (intrinsic viscosity 2.5 dL/g, 97% insoluble in *n*-heptane). The examined fiber samples, representative of significantly different conditions of structural disorder, were obtained by stretching strips of compression-molded sheets 1.35 mm thick, slowly crystallized from the melt (at 200 °C) under a press. They were drawn at a rate of 5 mm/min, with an initial length of 25 mm, in the ratio 3.0:1 under the following conditions: at 100 °C (sample 1); at 130 °C (sample 2);

Table 1. Parameters Used for Sample Preparation[a] and Apparent CrystalliteLengths along *a* and *b*, L_a and L_b,[b] for the Five Examined Samples Calculated According to Scherrer's Equation from the Half-Height Width of the Most Intense (110, 040, and 130) Equatorial Reflections

sample	DR	T_d (°C)	T_a (°C)	t_a (h)	L_a (Å)	L_b (Å)	$L_a = L_b$ (Å)
1	3:1	100	−	−	53 ± 3	51 ± 3	50
2	3:1	130	−	−	85 ± 11	101 ± 11	90
2′	3:1	130	160	12	82 ± 13	81 ± 9	80
3	3:1	130	172	64	127 ± 15	112 ± 13	120
3′	3:1	150	−	−	90 ± 13	101 ± 11	100

[a] DR, draw ratio; T_d, drawing temperature; T_a, annealing temperature; and t_a, the annealing time used for the preparation of the fiber samples. [b] The last column lists the values of L_a and L_b used in the reported calculations to be compared with the experimental profiles under the assumption $L_a = L_b$.

and at 130 °C, then being annealed at 172 °C for 64 h at a constant length (sample 3). Prompted by the results obtained for the above samples, two additional samples were also examined: a fiber drawn at 130 °C and annealed for 12 h at 160 °C (sample 2′) and a fiber drawn at 150 °C (sample 3′).

The 2D X-ray fiber diffraction patterns were obtained on a BAS-MS imaging plate (Fujifilm) using a cylindrical camera and were processed with a digital imaging reader (FUJIBAS 1800) (radiation used Cu Kα, monochromatized with a graphite single crystal or Ni-filtered).

The X-ray diffraction profiles on the first layer line were also collected using a Nonius CAD4 (four circles, K geometry) automatic diffractometer, with Ni-filtered Cu Kα radiation, with an equatorial geometry always maintained.[17] The reciprocal space corresponding to the reciprocal cylindrical coordinates $\zeta = 1/c = 0.154$ Å^{-1} and ξ in the range 0.20−0.55 Å^{-1} was sampled at steps of $\Delta\xi = 0.0033$ Å^{-1}. The Lorentz and polarization (Lp) correction is, according to the diffraction geometry, Lp $= (1 + \cos^2 2\theta)/\sin 2\theta$. It is worth noting that the use of the CAD4 diffractometer, which works at an enhanced distance between the sample and the detector (corresponding to 368 mm) with respect to the cylindrical camera used (with radius equal to 57.29 mm), ensures a better resolution in the collected diffraction patterns, although longer collection times are required. For the latter reason, we limited the automatic collection of the diffraction data to only the first layer line, where, as we shall see, the most significant fluctuations of the Bragg and diffuse scattering due to the presence of disorder have been observed.

The apparent crystallite lengths along *a* and along *b*, L_a and L_b, respectively, were estimated by measuring the half-height width of the 110, 040, and 130 diffraction peaks, i.e., the strongest intensity equatorial reflections, using Scherrer's formula. The values are reported in Table 1 for the five samples, which also reports the conditions under which the fibers were obtained. The values of L_a and L_b are nearly the same within the experimental error. Hence, for the sake of simplicity, in the reported calculations of the X-ray diffraction profiles to be compared with the experimental profiles, $L_a = L_b$ will be assumed, and the value used for these parameters is provided in the last column of Table 1.

Experimental Results

The X-ray diffraction photographs in two extreme cases, i.e., for sample 1 and sample 3, are reported for

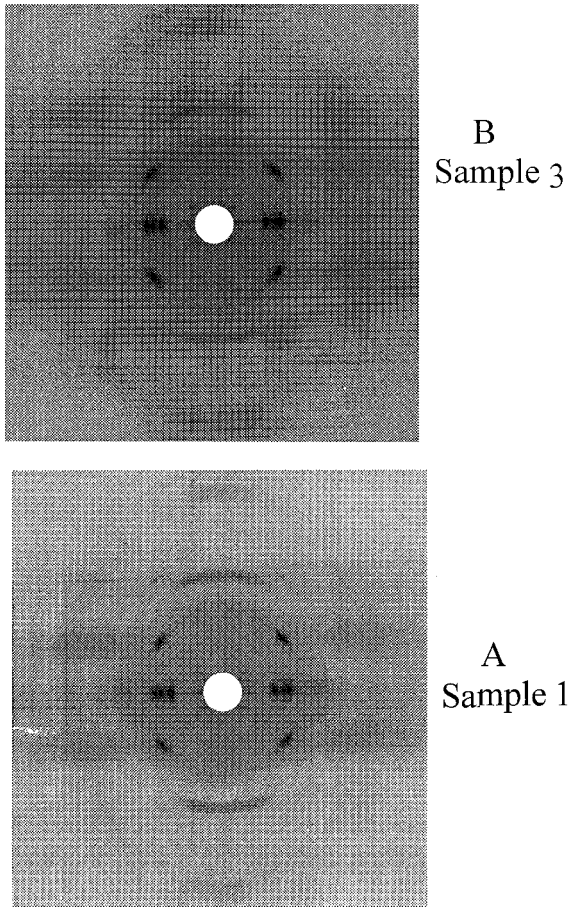

Figure 3. X-ray fiber diffraction patterns, taken on a photograph cylindrical camera, of i-PP (A) sample 1 and (B) sample 3. In B, Cu Kα radiation monochromatized with a graphite single crystal has been used.

comparison in Figure 3. In Figure 4A−C and 4A′−C′, the X-ray diffraction profiles read along the indicated layer lines of the photographic plates (Figure 3) are reported vs the reciprocal cylindrical coordinate ξ for the two samples. The *hkl* Miller indices of the diffraction peaks numbered in Figure 4 are indicated in Table 2. For sample 1, some *hkl* diffraction peaks, all with $h + k = 2n + 1$, are absent or very weak, whereas, for sample 3, they are narrow and sharp. The most drastic differences between the X-ray diffraction profiles of the two samples are observed along the first layer line, especially in the range 0.25 Å^{-1} < ξ < 0.55 Å^{-1} (see the insets in Figure 4B and B′), both for the intensities of the Bragg reflections and for the accompanying characteristic diffuse scattering,[18] which is much more prominent for sample 1. For example, in the case of sample 1, diffraction peaks 8 and 13, for which *hk*1 reflections with $h + k = 2n + 1$ mainly contribute (see Table 2), disappear almost completely. Diffraction peaks 9, 10, 12, and 16, for which *hk*1 reflections with $h + k$ equal to even and odd numbers both contribute, are noticeably reduced with respect to those of sample 3 (Figure 4B′). Finally, the X-ray diffraction profile of sample 1 for $l = 1$ in the ξ range 0.25−0.55 Å^{-1} presents a maximum of intensity corresponding to peak 11, characterized only by *hk*1 reflections with $h + k = 2n$, whereas, for sample 3, peaks 9, 10, and 12 are twice as intense as peak 11.

As we shall see, the distribution of X-ray diffraction intensity for samples drawn at low temperatures (such

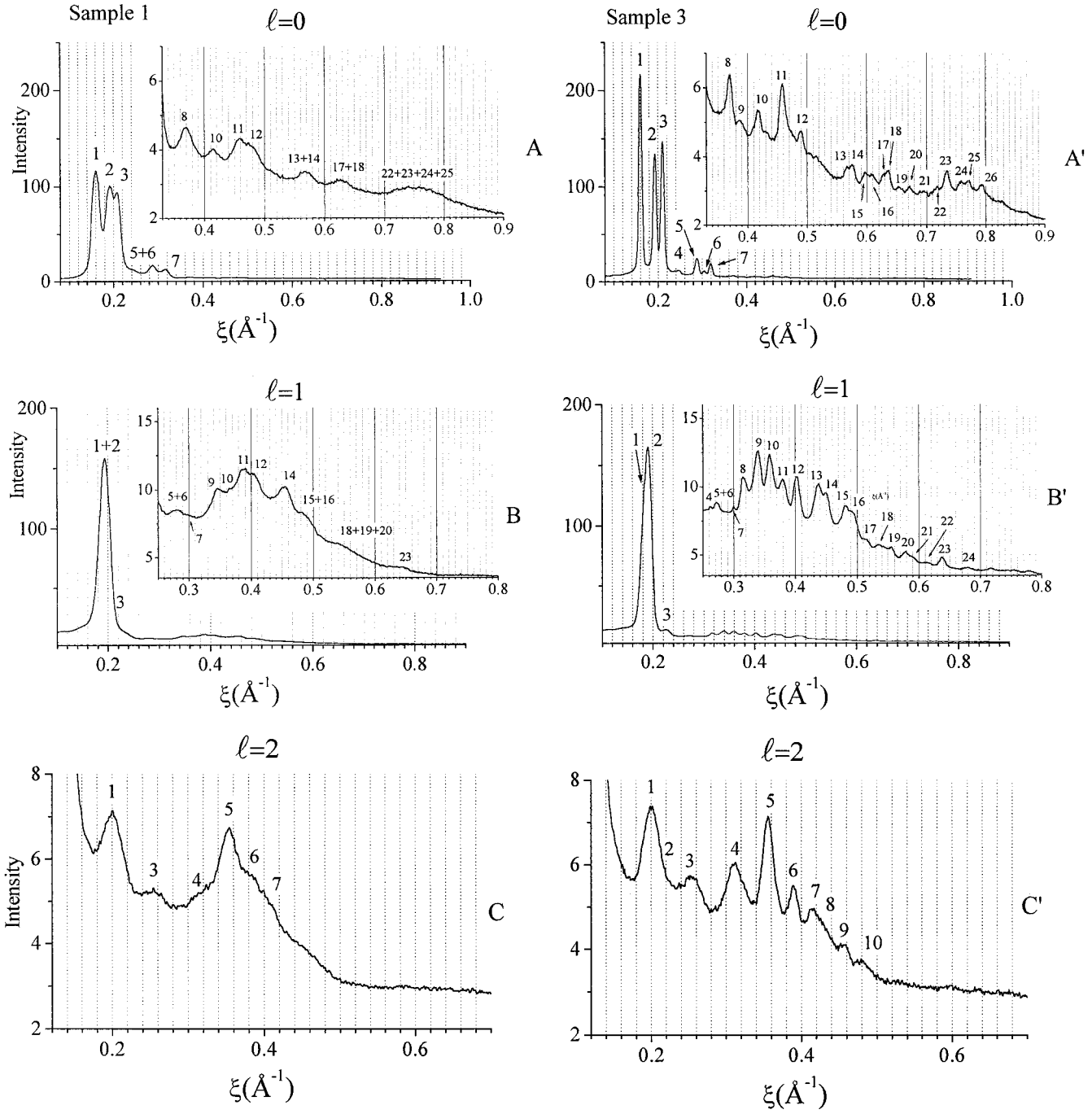

Figure 4. X-ray diffraction profiles vs the reciprocal cylindrical coordinate ξ, read along (A, A′) the equatorial, (B, B′) the first, and (C, C′) the second layer lines from the photographs of samples 1 and 3 of Figure 3. The diffraction peaks are numbered, and the Miller indices of the corresponding reflections are reported in Table 2.

as sample 1) can be accounted for by the space group C2/*c*,[1] implying a random positioning of up and down chains in the lattice. The intensities from drawn fibers annealed at temperatures close to the melting point (such as sample 3) will be explained, instead, by assuming that the lattice is not centered monoclinic, although the occurrence of a small percent of errors in the up/down setting of the helices in the lattice positions with respect to the limit-ordered model structure can not be excluded. This is indicated by the presence of a diffuse scattering subtending the Bragg reflections.

The X-ray diffraction patterns collected with an automatic diffractometer (at enhanced resolution) along the first layer line in the range 0.20 Å^{-1} < ξ < 0.55 Å^{-1} for samples 1, 2, and 3 are reported in Figure 5A, B, and C, respectively, after background subtraction (assumed as a straight line) and Lp correction. The numbers in the figure represent the *hk*1 Miller indices of the arrowed diffraction maxima, all with $h + k = 2n$. The vertical lines cross the diffraction maxima, which are strong and narrow for sample 3 but become weaker or almost absent for sample 2 and sample 1. The diffuse scattering subtending the Bragg reflections assumes characteristic shapes and increases with increasing disorder. It is worth noting the occurrence of a diffraction peak at ξ = 0.226 Å^{-1}, starred in Figure 5A−C (peak 3 in Figure 4B,B′ and in Table 2), which becomes

Table 2. *hkl* Miller Indices of the X-ray Diffraction Maxima Numbered in the Patterns of Figure 4A–C and 4A′–C′,[a] Observed Bragg Distances (d_o), Reciprocal Cyclindrical Coordinates (ξ_o), and Calculated Bragg Distances (d_c)

n	hkl	ξ_o (Å^{-1})	d_o (Å)	d_c (Å)	n	hkl	ξ_o (Å^{-1})	d_o (Å)	d_c (Å)	n	hkl	ξ_o (Å^{-1})	d_o (Å)	d_c (Å)	n	hkl	ξ_o (Å^{-1})	d_o (Å)	d_c (Å)
											$l = 0$								
1	110	0.160	6.25	6.27	11	270	0.459	2.18	2.20	17	430	0.628	1.59	1.60	24	500	0.758	1.32	1.31
2	040	0.193	5.18	5.18		300			2.19		390			1.59		510			1.31
3	130	0.210	4.76	4.76		310			2.18	18	440	0.639	1.56	1.57		520			1.30
4	140	0.246	4.07	4.07		190			2.17	19	2 12 0	0.654	1.53	1.53	25	0 16 0	0.772	1.29	1.30
5	150	0.289	3.46	3.51	12	280	0.490	2.04	2.03		450			1.53		530			1.29
	060			3.46		340			2.02	20	460	0.673	1.48	1.48		4 10 0			1.29
6	200	0.305	3.28	3.29	13	370	0.569	1.76	1.76		0 14 0			1.48		3 13 0			1.29
	210			3.25		2 10 0			1.75	21	1 14 0	0.697	1.43	1.44	26	540	0.794	1.26	1.27
7	220	0.319	3.13	3.13	14	0 12 0	0.579	1.73	1.73		470			1.44		2 15 0			1.27
8	240	0.368	2.72	2.78	15	380	0.599	1.67	1.67		2 13 0			1.43		1 16 0			1.27
	170			2.70		1 12 0			1.67		3 11 0			1.43		550			1.25
9	080	0.387	2.58	2.59	16	400	0.610	1.64	1.64	22	480	0.719	1.39	1.39					
	250			2.58		410			1.64										
10	180	0.419	2.39	2.41		2 11 0			1.63	23	3 12 0	0.733	1.36	1.36					
	260			2.38		420			1.62		1 15 0			1.35					
											2 14 0			1.35					
											$l = 1$								
1	111	0.181	4.21	4.20	11	241	0.379	2.44	2.44	17	1 10 1	0.515	1.86	1.87	22	391	0.614	1.58	1.58
2	131	0.190	4.06	4.04		171			2.44		291			1.85		441			1.58
	041			4.03		081			2.40		341			1.84		381			1.58
3	131	0.226	3.65	3.64	12	261	0.402	2.32	2.32	18	0 11 1	0.533	1.80	1.81	23	421	0.639	1.52	1.52
	141			3.59		181			2.30		351			1.79		1 13 1			1.52
4	141	0.262	3.29	3.30		251			2.30	19	291	0.553	1.74	1.77		2 12 1			1.51
5	151	0.271	3.20	3.19	13	091	0.438	2.15	2.17		1 11 1			1.76		391			1.50
6	211	0.285	3.09	3.09		311			2.16		371			1.75		3 10 1			1.50
	061			3.04		261			2.16		2 10 1			1.73		431			1.50
7	221	0.298	2.99	2.99		271			2.15		1 11 1			1.73		1 13 1			1.49
	151			2.98		321			2.13		361			1.72		461			1.49
8	161	0.315	2.85	2.85	14	331	0.460	2.07	2.08	20	0 12 1	0.579	1.67	1.67	24	471	0.670	1.45	1.44
	231			2.84		191			2.03		381			1.67		0 14 1			1.44
9	071	0.340	2.68	2.69	15	0 10 1	0.481	1.98	1.97		2 10 1			1.66		451			1.44
	161			2.68		311			1.98		411			1.65					
	241			2.69		321			1.94		371			1.65					
	221			2.67		351			1.93	21	421	0.593	1.63	1.63					
10	231	0.358	2.57	2.57	16	1 10 1	0.492	1.94	1.91		1 12 1								
	171			2.55		331			1.91										
						281			1.89										
											$l = 2$								
b	102	0.095	3.10	3.08	4	162	0.308	2.30	2.35	6	232	0.389	2.02	2.05	9	342	0.458	1.81	1.83
	022			3.07		062			2.34		262			2.02		262			1.82
	112			3.04		232			2.30		082			2.02	10	352	0.480	1.75	1.77
1	042	0.205	2.70	2.73		152			2.28		172			2.01		192			1.76
	102			2.73		242			2.25	7	302	0.417	1.93	1.95		272			1.74
	112			2.71	5	202	0.355	2.13	2.14		312			1.94		1 10 2			1.72
2	142	0.220	2.64	2.64		162			2.14	8	322	0.430	1.89	1.92					
	122			2.64		252			2.14		272			1.92					
3	052	0.251	2.51	2.54		172			2.13		252			1.90					
	132			2.54		212			2.13		332			1.88					
	202			2.49							092			1.88					
	212			2.48							182			1.87					
	152			2.47															

[a] The subscripts o and c stand for "observed" and "calculated" parameters. The unit cell parameters have been fixed according to those of Hikosaka and Seto (ref 3), i.e. $a = 6.65$ Å, $b = 20.73$ Å, $c = 6.50$ Å, and $\beta = 98.67°$. [b] This peak has not been included in the profiles of Figure 4C and 4C′.

progressively less pronounced with the increasing structural disorder of the i-PP samples. The reflection mainly contributing to this maximum is the 131 (with $h + k = 2n$), rather than the $\bar{1}41$ (with with $h + k = 2n + 1$; see, for example, Table A in ref 2). Hence, the apparent decrease of the intensity of this peak can not be ascribed to the increasing degree of disorder in the examined i-PP samples; it is probably partially due to the progressive decrease in the crystallite size going from sample 3 to sample 1, which, in turn, produces a progressive increase in the half-height width of the diffraction peaks. Indeed, for sample 1, for which the values of L_a and L_b have been estimated to be on the order of 50 Å, peak 3 appears just as a shoulder of the strong diffraction peak 2 (see Figures 5A and 4B). More accurate structure-refining procedures than those reported in the past literature are probably needed to clarify this and other aspects of the experimental diffraction pattern of the most ordered modification of α i-PP.

Figure 6A,B reports the X-ray diffraction profiles along the first layer line vs ξ for samples 2′ and 3′ after background subtraction (assumed to be a straight line) and Lp correction, as recorded with the imaging plate system. As we will see in a next section, sample 2′ is in a modification more ordered than the modification of sample 2 but less ordered than that of sample 3, whereas sample 3′ is probably a mixture of crystals in modifications very close to the limit-ordered and -disordered model structures. Probably the most ordered crystals are formed under drawing conditions at 150 °C,

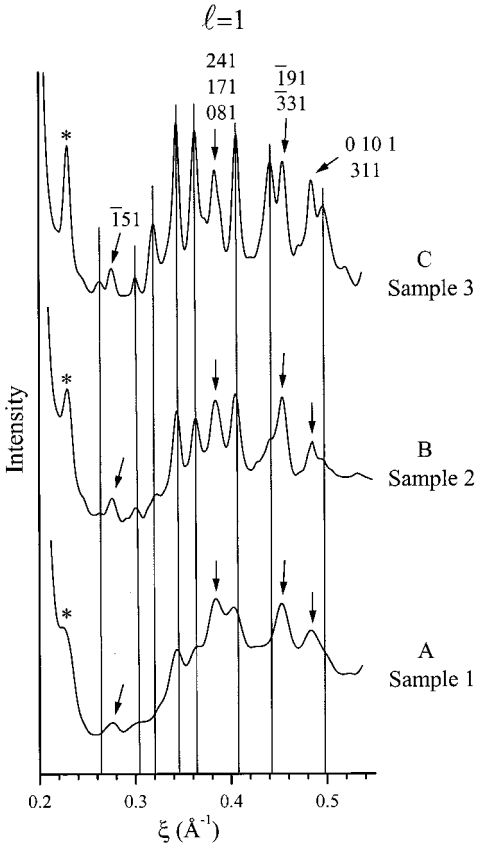

Figure 5. X-ray diffraction profiles recorded on the first layer line with an automatic diffractometer in the reciprocal space zone $\zeta = 1/c$, 0.20 Å^{-1} < ξ < 0.55 Å^{-1} of samples 1, 2, and 3 after subtraction of a straight baseline and Lp correction.

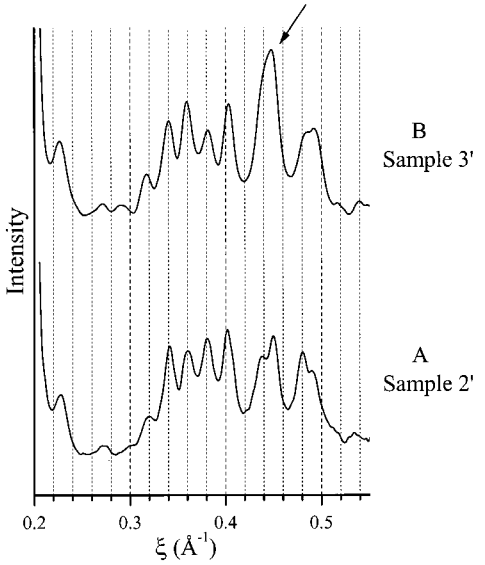

Figure 6. X-ray diffraction profiles read from the photograph imaging plates along the first layer line in the reciprocal space zone $\zeta = 1/c$, 0.20 Å^{-1} < ξ < 0.55 Å^{-1} of samples (A) 2′ and (B) 3′ after subtraction of a straight baseline and Lp correction. For the arrowed maximum, see the text.

whereas the more disordered ones are formed upon cooling of the sample to room temperature.

It is worth noting, for sample 3′, the appearance of a strong anomalous intensity maximum centered around $\xi = 0.45$ Å^{-1} (arrowed in Figure 6B). This is due to the presence of a non-negligible amount of daughter lamellae tilted by ∼80° with respect to the parent lamellae, the *c* axes of the latter being parallel to the *a* axis of the former.[19−22] The growth of branched lamellae in oriented as well unoriented i-PP samples is well documented in the literature (see, for example ref 10 and references therein), and it manifests itself in the X-ray diffraction pattern of fiber samples, especially with the presence of a strong nearly meridional maxima on the first layer line, due to the 110 reflection diffracted from the lamellae tilted with the *c* axes ∼80° from the fiber axis. We have verified the presence of such strong intensity on the meridian for our samples in the X-ray photographs (not shown here). The anomalous strong maximum on the first layer line (arrowed in Figure 6) is due to the strong 013 + $\bar{1}$13 and 023 + $\bar{1}$23 reflections (d = 2.09 and 2.13 Å, respectively) on the third layer line, which for the tilted lamellae, are rather arced and are manifested around $\xi = 0.45$ Å^{-1} on the first layer line, and around $\xi = 0.47$ Å^{-1} on the equatorial layer line.

Calculation Methods

The average X-ray diffraction intensity along the layer lines is calculated as the sum of a Bragg contribution (comprising the broadening effect of the reflections as well as the background contribution due to the finite dimensions of the crystallites) and a diffuse contribution due to the occurrence of long-range disorder, according to the standard formula[18]

$$I(\xi,\zeta) = |G|^2 <|F|>^2 + <N^2>/\langle N\rangle\,(<|F|^2> - <|F|>^2) \quad (1)$$

where $<|F|>^2$ and $<|F|^2>$ are the square of the mean modulus and the mean square modulus, respectively, of the structure factor of the repeating motif (i.e., the unit cell, the *a*−*c* bilayer, or a cluster of first-neighbor i-PP chains in the α form). A Bernoulli-type distribution of the size of the crystallites is assumed; accordingly, $|G|^2$ corresponds to the square of the Laue function for a single crystal and is the product of terms of the kind[23]

$$|G_x|^2 = (1 - p^2{}_x)/[1 + p^2{}_x - 2\,p_x \cos(2\pi s_x x)] \quad (2)$$

with $1 - p_x$ representing the probability that a crystallite terminates growth along the lattice direction x (*a*, *b* or *c*), assumed independent of the length of the crystallite itself, and s_x is the component of the scattering vector s (= 2 sin θ/λ) along the reciprocal direction x* (*a**, *b** or *c**). $<N>$ and $<N^2>$ are the mean number and the mean square number, respectively, of the repeating motifs along the lattice directions. According to Ruland (see, for example, ref 24 and note 25), p_x is related to the apparent length of the crystallites along the x lattice direction, L_x, through eq 3.

$$p_x = \exp(-2x/L_x) \quad (3)$$

As already stated at the end of the Experimental Section, in the calculated profiles to be compared to the experimental ones for the various samples, the values of L_a and L_b were fixed equal to the values listed in the last column of Table 1 (in the approximation $L_a = L_b$), whereas the dimensions of the crystalline domains along *c* were considered infinite. Including a finite value of L_c in the calculation, indeed, would imply a multiplication of the calculated intensities along the layer lines for a constant value. In all reported calculations, the intensities were normalized by a factor leading to an

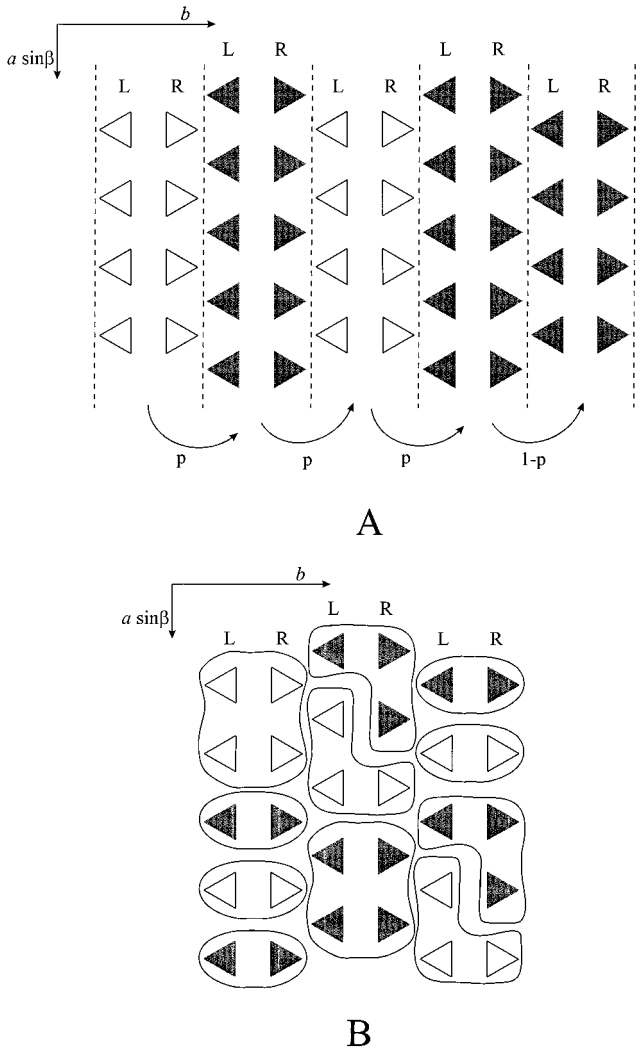

Figure 7. Models of possible packing of right- (R) and left- (L) handed 3/1 helices of i-PP. (A) A bilayer of macromolecules is juxtaposed along *b* to a bilayer of anticlined macromolecules (as in the space group $P2_1/c$) with probability p and to a bilayer of isoclined macromolecules (as in the space group $C2/c$) with probability $(1 - p)$. (B) Small clusters (enclosed in a loop) of isoclined chains belonging to the same bilayer are packed, both along *a* and *b*, with equal probability with clusters of chains having the same or opposite orientation with respect to the chains of the cluster in question. The different up/down orientations of the chains are indicated by filled and open triangles.

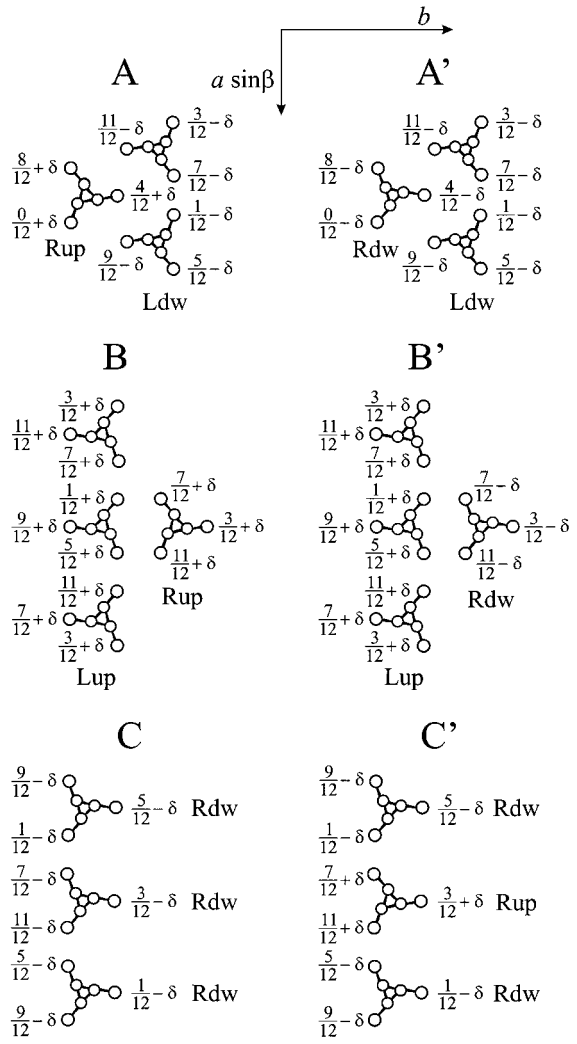

Figure 8. Packing situations arising from the facing of i-PP helices according to the space group $P2_1/c$ (A, B, C) and assuming the wrong up/down orientation for one of them (A′, B′, C′). (A′) The packing error occurs along *b* at the interface between adjacent bilayers. (B′) The packing error occurs along *b* at the interface of *a*-*c* layers within a bilayer. (C′) The packing error occurs along *a* within an *a*−*c* layer. The orthogonal coordinates of the methyl groups with respect to a frame having *z* and *y* coinciding with *c* and *b* of the unit cell are indicated, δ being the increment to the *z* atomic coordinates. $\delta = 0$ implies that the positions of the methyl carbon atoms of isomorphous anticlined helices coincide.

equal value of the integrated intensity regardless of the assumed dimensions of the crystallites. For the sake of simplicity, the atomic coordinates and the unit cell parameters were fixed equal to those refined in the model of i-PP in the limit-ordered structure $P2_1/c$ by Hikosaka and Seto in ref 3. Moreover, the reported calculations are relative to the first layer line only, where the most significant fluctuations of the Bragg and the diffuse scattering due to the presence of disorder have been observed (see Experimental Results).

The packing energy has been evaluated as one-half of the sum of the interaction energies between the atoms of a given helix with the those of the surrounding helices. The interactions were calculated within spheres of radii equal to twice the sum of the van der Waals radii for each pair of atoms. The nonbonded energy functions with the parameters reported by Flory and co-workers in ref 26 are used. The energy calculations were performed using either the fractional coordinates and unit cell parameters of the refined model by Hikosaka and Seto[3] or the coordinates of the minimum conformational energy situation and the unit cell parameters of refs 27 and 28. No significant differences were found; therefore, only the results of the packing energy calculations relative to the first case are reported.

Results and Discussion

Possible Models of Long-Range Disorder and Packing Energy Cost of the Defects. The first model of long-range disorder considered here is of the kind already discussed by Corradini et al.,[16] cited in the Introduction. In each bilayer, the macromolecules are supposed to be all isoclined (as in the space group $P2_1/c$). Disorder arises for macromolecules belonging to adjacent bilayers stacked along *b*, which can be isoclined or anticlined. More precisely, a bilayer of macromol-

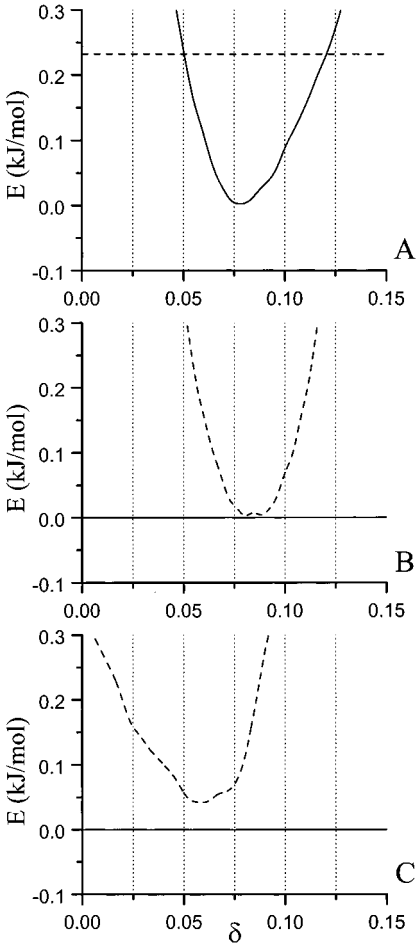

Figure 9. Packing energy E per mole of monomeric units as a function of δ for the situations of Figure 8 A−C (solid lines) and Figure 8 A′−C′ (dashed lines).

ecules is juxtaposed to a bilayer of anticlined macromolecules (as in the space group $P2_1/c$) with probability p and to a bilayer of isoclined macromolecules with probability $(1 - p)$, see Figure 7A. Because of the presence of such errors, the local arrangement of the chains arising at the interface between two consecutive bilayers is as illustrated in Figure 8A′, for example, which is compared with the ordered packing situation in the space group $P2_1/c$ (Figure 8A). In Figure 8, the z/c orthogonal coordinates of the methyl groups, in a reference frame having the z and y axes coinciding with c and b of the unit cell in the limit-ordered model structure, respectively, are indicated. δ is the increment to the z atomic coordinates, whose value was set equal to zero in the original model of Natta and Corradini,[1] whereas $\delta = 0.07$ in the refined $P2_1/c$ packing model proposed by Hikosaka and Seto.[3] When $\delta = 0$, the position of the methyl groups of two anticlined isomorphous chains vicariously substituting one each other in the same lattice position coincides.

In Figure 9A, the packing energy E per mole of monomeric units is calculated as a function of δ, for the two schemes of Figure 8A (solid line) and 8A′ (dashed line). In the latter case, the packing energy does not depend on the δ value, of course. For the packing scheme of Figure 8A, instead, as already calculated in ref 16, a flat minimum occurs for a value of δ close to the refined one proposed by Hikosaka and Seto.[3] The energy cost of defects of the kind indicated in Figure 8A′ is very low, on the order of 0.23 kJ/mol of monomeric units.

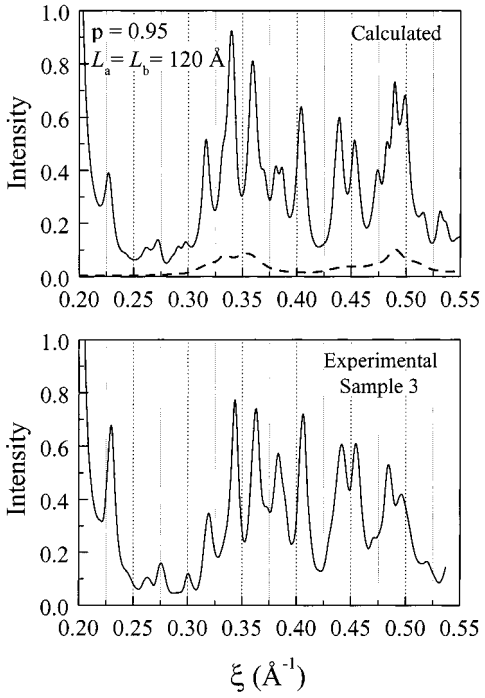

Figure 10. The experimental X-ray diffraction pattern of sample 3 of Figure 5C is compared with the calculated X-ray diffraction profile on the first layer line for a model structure comprising 5% of bilayers with a wrong up/down orientation with respect to the limit-ordered model structure ($P2_1/c$, α_2 form). The perfect orientational up/down order is maintained inside the bilayers (see Figure 7A). L_a and L_b are the apparent sizes of the crystallites along a and along b (a Bernoulli-type distribution of the sizes of the crystallites is assumed). The dashed lines indicate the diffuse scattering contribution due to the occurrence of the disorder, the solid lines the sum of the latter and the Bragg contributions.

It is worth noting that these kinds of defects are in line with the chain-folding scheme proposed by Petraccone et al. in refs 29 and 30. On the basis of simple configurational considerations, they established that the folding occurs between enantiomorphous isoclined chains, with the hypothesis of adjacent re-entry chain folding. Hence, in i-PP crystals very close to the limit-ordered structure, the chain folding should occur only between first-neighbor chains belonging to a bilayer, the folding plane being the (010), in agreement with morphological experimental evidence.[31−33] In the chain-folding model of refs 29 and 30, the folding directions are alternatively parallel to the (100) and (140) [or (100) and (1$\bar{4}$0)] crystallographic planes. This chain-folding scheme is, therefore, compatible not only with the perfect packing scheme of the limit-ordered modification, but also with situations of disorder, insofar as the up/down disorder is assumed to occur in the stacking along b of perfectly ordered bilayers.

We have also considered the possibility of occurrence of the up/down disorder within a bilayer, either along b or along a. In Figure 8B′ and 8C′, the situations that arise from the wrong up/down orientation of a chain facing along b to an $a-c$ layer without defects within a bilayer (Figure 8B′) or of a helix along a (Figure 8C′) are illustrated and compared to the canonical packing situation occurring in the $P2_1/c$ space group symmetry (Figure 8B and 8C, respectively). In Figure 9B and 9C, the calculated packing energy E (per mole of monomeric units) as a function of δ in the case of Figure 8B and 8C (solid line) and of Figure 8B′ and 8C′ (dashed line)

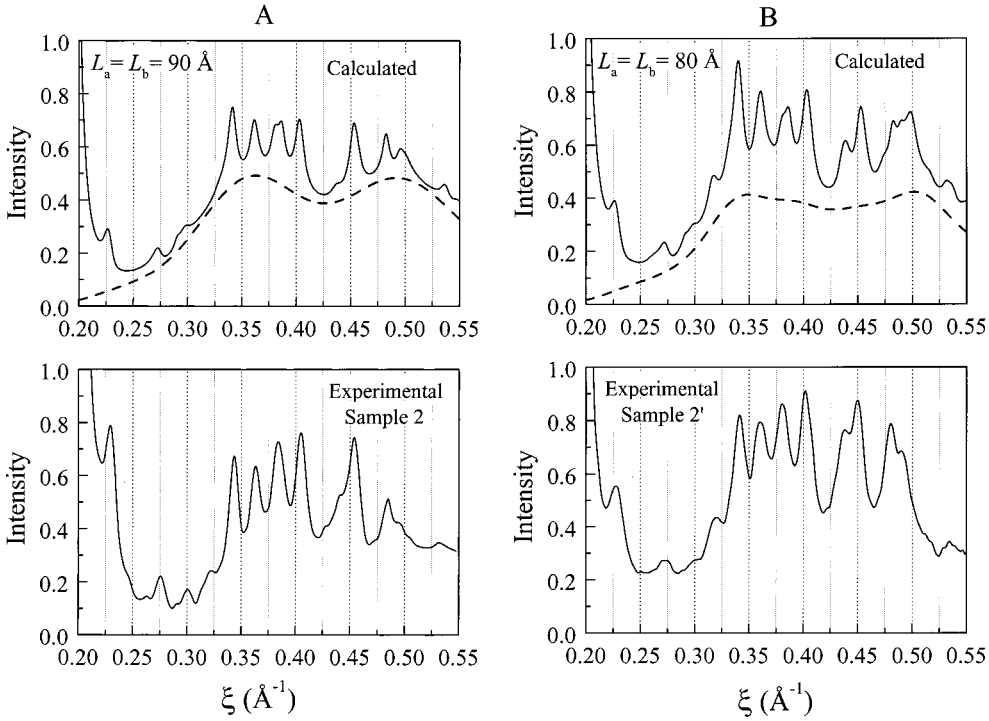

Figure 11. (A) The experimental X-ray diffraction profile of sample 2 of Figure 5B is compared with the calculated X-ray diffraction profile on the first layer line for a model structure in which small clusters of 2−3 isoclined chains belonging to the same bilayer, are facing, both along *a* and along *b*, with equal probability, toward clusters of chain having the same or opposite orientation with respect to the chains of the cluster in question (see Figure 7B). (B) The experimental X-ray diffraction profile of sample 2′ of Figure 6A is compared with the calculated X-ray diffraction profile on the first layer line for a model structure with the clusters made up of four chains; in 70%, the up/down setting of the chains in the cluster is the same as in the limit-ordered model structure, in the remaining 30%, the clusters are disordered in the relative up/down orientations of the chains. L_a and L_b are the apparent sizes of the crystallites along *a* and along *b* (a Bernoulli-type distribution of the sizes of the crystallites is assumed). The dashed lines indicate the diffuse scattering contribution due to the occurrence of the disorder, the solid lines the sum of the latter and the Bragg contributions.

are reported. Of course, the value of E does not depend on δ in the canonical $P2_1/c$ case, whereas it presents a very flat minimum in the defective cases of Figure 8B′ and 8C′. Also, in these cases, the minima correspond to a δ value close to the refined value of ref 3. The energy cost of the defect of Figure 8B′ is about zero; it amounts to less than 0.1 kJ/mol of monomeric units in the case of the defect of Figure 8C′. From these data, it is reasonable to suppose that, under conditions of fast crystallization, the chain folding may not develop according to a well-defined pattern within the bilayers and the up/down disorder may arise also within the bilayers both along *b* and along *a*. As a result, disordered structures close to the limit-disordered model are formed at low crystallization temperatures. A possible model in which small clusters of all up or all down chains, belonging to a same bilayer, are faced at random with clusters of isoclined or anticlined chains with respect to the chains of the cluster in question is shown in Figure 7B as an example.

Comparison between the Calculated and Experimental X-ray Diffraction Profiles ($l = 1$). In the following, we compare the most significant experimental intensity profiles (those for $l = 1$) with appropriate calculations corresponding to various amounts of long-range disorder.

In Figures 10−13, calculated X-ray diffraction intensity profiles for the first layer line ($\zeta = 1/c = 0.1538$ Å^{-1}), for different kinds and amount of disorder, are compared with the experimental patterns of samples 3 (Figure 10), 2 and 2′ (Figure 11A and 11B, respectively), 1 (Figure 12), and 3′ (Figure 13). The apparent sizes of the crystallites along the *a* and *b* directions, L_a and L_b, respectively, are indicated. The dotted lines correspond to the calculated diffuse scattering contribution due to the disorder, whereas the solid lines are the sum of the latter with the Bragg contribution.

The features of the experimental X-ray diffraction profile of sample 3 are best reproduced by the profile calculated for a model structure very close to the limit-ordered one, but for the inclusion of 5−10% of errors in the relative up/down orientation of consecutive perfectly ordered bilayers piled along *b* (see Figure 7A); the calculation for the case of 5% ($p = 0.95$, Figure 7A) is shown, as an example, in Figure 10. This result is in line with the model of chain folding proposed by Petraccone et al.[29,30]

In the case of sample 2 (drawn at 130 °C), the kind of disorder discussed above is insufficient to explain the diffuse X-ray diffraction pattern even if it is assumed to be complete ($p = 0.50$, Figure 7A). A satisfactory agreement with the experimental data is obtained with the hypothesis that small clusters of 2−3 isoclined chains belonging to the same bilayer are packed, both along *a* and along *b*, with equal probability with clusters of chains having the same or opposite orientation with respect to the chains of the cluster in question (see Figure 7B). The calculated X-ray diffraction profile for the indicated values of L_a and L_b is reported in Figure 11A.

A less disordered model structure suffices to explain the main diffraction features of sample 2′, a fiber drawn

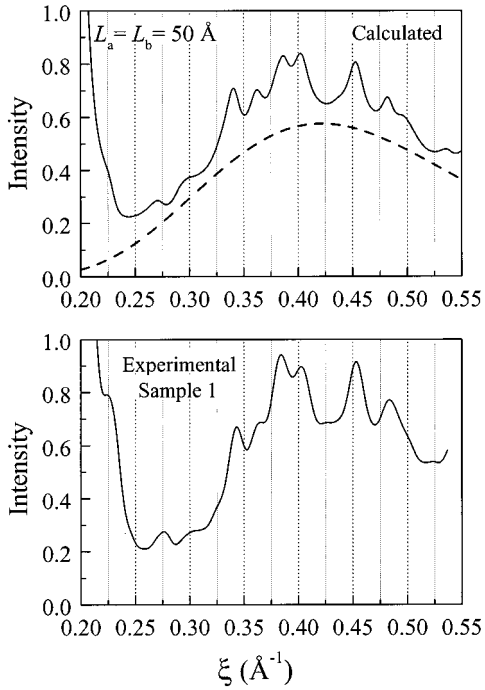

Figure 12. The experimental X-ray diffraction profile of sample 1 of Figure 5A is compared with the calculated X-ray diffraction profile on the first layer line for the limit-disordered model structure of Figure 2B. L_a and L_b are the apparent sizes of the crystallites along *a* and along *b* (a Bernoulli-type distribution of the sizes of the crystallites is assumed). The dashed lines indicate the diffuse scattering contribution due to the occurrence of the disorder, the solid lines the sum of the latter and the Bragg contributions.

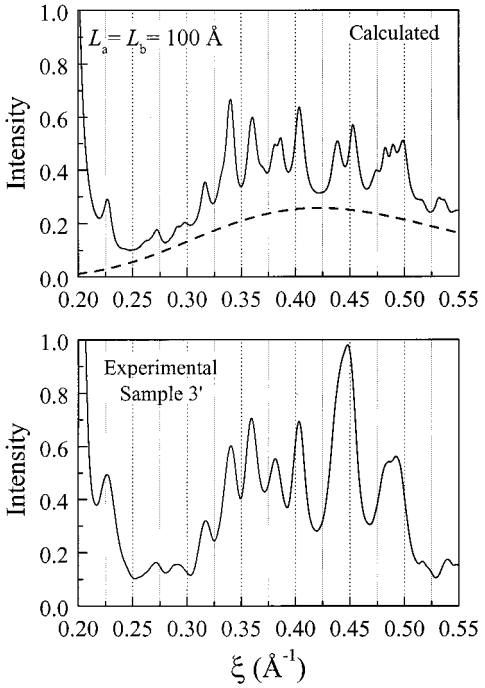

Figure 13. The experimental X-ray diffraction profile of sample 3′ of Figure 6B is compared with the X-ray diffraction profile of the first layer line obtained by weight averaging at 50%, as an example, those calculated for the two limit-ordered (Figure 2A) and limit-disordered (Figure 2B) model structures. L_a and L_b are the apparent sizes of the crystallites along *a* and along *b* (a Bernoulli-type distribution of the sizes of the crystallites is assumed). The dashed lines indicate the diffuse scattering contribution due to the occurrence of the disorder, the solid lines the sum of the latter and the Bragg contributions.

at 130 °C and then annealed for 12 h at 160 °C (see Figure 11B). For example, the calculated diffraction profile of Figure 11B is relative to a model structure in which the clusters are made up of four chains, whereby in 70%, the up/down setting of the chains is the same as in the limit-ordered model structure, and in the remaining 30%, the clusters are disordered in the relative up/down orientations of the chains. It is likely that samples not subjected to annealing treatments at temperatures close to the melting point may not develop chain-folding patterns of the kind described in refs 29 and 30 for kinetic reasons. Hence, the up/down disorder is present within the bilayers.

In the case of sample 1, drawn at 100 °C, the shape of the diffuse scattering (Figure 12) is best reproduced with the hypothesis that each lattice site is occupied with equal probability by up or down chains, as in the limit-disordered model structure (Figure 2B). We cannot exclude the occurrence of local correlations in the relative up/down orientation of first-neighbor helices, of course, tending to favor the facing of isoclined chains within the bilayers, but in this case, the correlations should develop at very short range.

Finally, sample 3′ (a fiber drawn at 150 °C, with no annealing) is probably a mixture of crystals very close to the limit-ordered and the limit-disordered model structures, as shown in Figure 13, where the experimental X-ray diffraction profile along the first layer line of the sample is compared to that obtained by weight averaging at 50%, as an example, those calculated for the two limit-ordered and limit-disordered model structures.

The occurrence of up/down disorder within the bilayers in drawn, but not annealed, fibers is associated with the kinetic preclusion for the formation of regularly folded crystals and may thus be concomitant with the presence of a more relevant fraction of tie chains between crystals. The effect on the fiber properties might be significant.

Conclusions

In this paper, a detailed analysis of the Bragg as well as of the diffuse X-ray diffraction scattering of i-PP fiber samples, suitably crystallized under different conditions, is performed. The fiber samples typically crystallize in the α form, involving various degrees of disorder, depending on the mechanical and thermal history of the samples, and varying from sample to sample. We have chosen samples representative of limiting cases of long-range disorder, spanning from a limit-ordered to a limit-disordered model structure. The experimental X-ray diffraction patterns are compared with those calculated for model structures involving various degrees and kinds of up/down disorder.

The samples slowly crystallized at high temperatures, near to the melting temperature, approach thermodynamic equilibrium and correspond to packing situations very close to those of the limit-ordered model structure ($P2_1/c$, α_2 form); only 5−10% of defects in the relative orientation of consecutive bilayers along *b* is left, within this scheme, and perfect order is maintained inside the bilayers. This unidimensional model of disorder is consistent with the chain-folding scheme, proposed in the literature,[29,30] based on simple configurational and crystallographic considerations. According to this model, which hypothesizes adjacent re-entry, the chain folding

can occur only between enantiomorphous isoclined chains, i.e., within bilayers ordered according to the limit-ordered model structure.

For samples crystallized far from the thermodynamic equilibrium, the chain folding can not develop according to a well-defined pattern, for kinetic reasons, so that the up/down disorder occurs also within the bilayers both along *b* and along *a*. Situations close to the limit-disordered model structure (C2/*c*, α_1 form) might arise at the lower crystallization temperatures; we have seen that this occurs at a low cost of packing energy.

Acknowledgment. This work was supported by the Ministero dell'Università e della Ricerca Scientifica e Tecnologica (PRIN 1998 titled "Stereoselective Polymerization: New Catalysts and New Polymeric Materials"). Polypropylene samples were provided by Montell Polyolefins. X-ray diffraction data were recorded with a Nonius CAD4 automatic diffractometer (Centro Interdipartimentale di Metodologie Chimico Fisiche, Universiy of Naples).

References and Notes

(1) Natta, G.; Corradini, P. *Nuovo Cimento Suppl.* **1960**, *15*, 40.
(2) Mencik, Z. *J. Macromol. Sci. Phys.* **1972**, *6*, 101.
(3) Hikosaka, M.; Seto T. *Polym. J.* **1973**, *5*, 111.
(4) Immirzi, A.; Iannelli, P. *Macromolecules* **1988**, *21*, 768.
(5) Brückner, S.; Meille, S. V. *Nature* **1989**, *340*, 455.
(6) Ferro, D. R.; Brückner, S.; Meille, S. V.; Ragazzi, M. *Macromolecules* **1992**, *25*, 5231.
(7) Meille, S. V.; Ferro, D. R.; Brückner, S.; Lovinger, A. J.; Padden, F. J. *Macromolecules* **1994**, *27*, 2615.
(8) Dorset; D. L.; McCourt, M. P.; Kopp, S.; Schumacher, M.; Okihara, T.; Lotz, B. *Polymer* **1998**, *25*, 6331.
(9) Corradini, P.; Petraccone, V.; De Rosa, C.; Guerra, G. *Macromolecules* **1986**, *19*, 2699.
(10) Brückner, S.; Meille, S. V.; Petraccone, V.; Pirozzi, B. *Prog. Polym. Sci.* **1991**, *16*, 361.
(11) Corradini, P.; Guerra, G. *Adv. Polym. Sci.* **1992**, *100*, 183.
(12) IUPAC Commission on Macromolecular Nomenclature. *Pure Appl. Chem.* **1981**, *53*, 733.
(13) Guerra, G.; Petraccone, V.; Corradini, P.; De Rosa, C.; Napolitano, R.; Pirozzi, B.; Giunchi, G. *J. Polym. Sci.: Polym. Phys.* **1984**, *22*, 1029.
(14) De Rosa, C.; Guerra, G.; Napolitano, R.; Petraccone, V.; Pirozzi, B. *Eur. Polym. J.* **1984**, *20*, 937.
(15) De Rosa, C.; Guerra, G.; Napolitano, R.; Petraccone, V.; Pirozzi, B. *J. Therm. Anal.* **1985**, *30*, 1331.
(16) Corradini, P.; Giunchi, G.; Petraccone, V.; Pirozzi, B.; Vidal, H. M. *Gazz. Chim. Ital.* **1980**, *110*, 413.
(17) In the equatorial geometry, the X-ray diffraction intensity of each point in the reciprocal space is collected by placing the point in a horizontal plane (the *XY* plane in the *K* geometry) and moving the detector along the 2θ circle (also placed in the *XY* plane).
(18) Tadokoro, H. *Structure of Crystalline Polymers*; John Wiley & Sons: New York, 1979; pp 145−150.
(19) Khoury, F. *Bull. Am. Phys. Soc.* **1964**, *9*, 275. Khoury, F. *J. Res. Natl. Bur. Stand.* **1966**, *A70*, 29.
(20) Sauer, J. A.; Morrow, D. R.; Richardson, G. C. *J. Appl. Phys.* **1965**, *36*, 3017.
(21) Padden, F. J., Jr.; Keith, H. D. *J. Appl. Phys.* **1966**, *37*, 4013.
(22) Lotz, B.; Wittmann, J. C. *J. Polym. Sci.: Polym. Phys.* **1986**, *24*, 1541.
(23) Allegra, G.; Bassi, I. *Gazz. Chim. Ital.* **1980**, *110*, 437.
(24) Liu, X. D.; Ruland, W. *Macromolecules* **1993**, *26*, 3030.
(25) On p 2031 of ref 24, a parameter *H* is defined, having the same role as our p_x parameter when σ_3, i.e., the variance of the repetition unit length along a lattice direction numbered 3 in a paracrystal is set equal to zero. It is worth noting that the apparent length of the crystallites along the *x* lattice direction (L_x) is about twice the average dimensions of the crystallites for a Bernoulli-type distribution of the size ($x/(1 - p_x)$, as shown by Allegra in the paper *Acta Crystallogr.* **1982**, *A28*, 863.
(26) Yoon, D. Y.; Sundararajan, P. R.; Flory, P. J. *Macromolecules* **1975**, *8*, 776.
(27) Corradini, P.; Petraccone, V.; Pirozzi, B. *Eur. Polym. J.* **1976**, *12*, 831.
(28) Corradini, P.; Petraccone, V.; Pirozzi, B. *Eur. Polym. J.* **1983**, *19*, 299.
(29) Petraccone, V.; Pirozzi, B.; Meille, S. V. *Polymer* **1986**, *27*, 1665.
(30) Petraccone, V.; Pirozzi, B.; Meille, S. V. *Eur. Polym. J.* **1989**, *25*, 43.
(31) Martuscelli, E.; Pracella, M.; Zambelli, A. *J. Polym. Sci.: Polym. Phys.* **1981**, *18*, 619.
(32) Wittman, J. C.; Lotz, B. *J. Polym. Sci.: Polym. Phys.* **1985**, *23*, 205.
(33) Lotz, B.; Graf, S.; Wittman, J. C. *J. Polym. Sci.: Polym. Phys.* **1986**, *24*, 2017.

MA0002895